Trans Indian Inst Met (2015) 68(1):117–128
DOI 10.1007/s12666-014-0435-2

TECHNICAL PAPER

TP 2838

High Strength High Carbon Low Alloy Pearlite-Ferrite-Tempered Martensite Steels

A. Varshney · D. Verma · S. Sangal · K. Mondal

Received: 10 February 2014 / Accepted: 15 July 2014 / Published online: 15 October 2014

Abstract High strength multiphase steels have been developed consisting of combination of pearlite, tempered martensite and small amount of ferrite, by suitable heat treatment of a high carbon low alloy rail steel (0.7 % C). The desired microstructure has been obtained by holding fully homogenized steel in pearlitic range for small durations followed by water quenching and subsequent tempering at 773 K for 18 h. Variation in mechanical properties has been studied with the change in volume fraction of different phases. Yield strength, ultimate tensile strength and elongation are observed to be in the range of 500–1,000 MPa, 900–1,185 MPa and up to 16.8 %, respectively. Continuous and discontinuous yielding along with substantial work hardening has been explained as a function of tempered martensite content.

Keywords Electron microscopy · Mechanical characterization · Steel · Martensite

1 Introduction

Designing and developing cost effective steels with cheaper alloying elements for better mechanical properties have been a challenge for their structural applications. In view of these, many alloy steels have been developed like Transformation Induced Plasticity (TRIP) and Maraging steels [1, 2]. Though, these steels possess better mechanical properties in terms of tensile strength and toughness, but find special applications due to costly alloying additions. Hence, there have been constant efforts to design cost effective routes to develop structural alloy steels with improved strength and ductility and studies have been carried out to develop better structural steels by investigating the effect of volume fraction and distribution of constituent phases on the mechanical properties [3–19].

In particular, ferrite martensite dual phase (FMDP) steels have been developed by inter-critical annealing of conventional mild steel in two phase ($\gamma + \alpha$) region to obtain varying amount of ferrite. After that, the steel has been quenched for transformation of residual austenite to martensite [2–11]. Studies have since been carried out on the structure–property correlations for this class of steels.

Tamura et al. [3] have proposed empirical relations between volume fraction and flow stresses in ferrite-martensite mixture. They have concluded that dual phase steels follow law of mixtures linearly or non-linearly depending on the ratio of yield strength of martensite to that of ferrite. Based on the results of Tamura et al. [3], other investigators [5, 6] have analyzed and modified these relations.

Davies [5] and Araki et al. [8] have concluded that both uniform and total elongation would decrease non-linearly with volume fraction of martensite. Speich and Miller [6] as well as Eldis [9] have observed substantial increase in elongation of the steel containing high volume fraction of retained austenite. Becker and Hormbogen [10] have outlined the importance of distribution of martensite in the FMDP steels. It has also been reported that improvement in impact toughness relates to the change in distribution of phases [11, 12]. Other studies [13–15] have shown substantial work hardening behavior of the FMDP steels.

In recent years, different combinations of other constituent phases, like ferrite and bainite in Ferrite Bainite Dual Phase (FBDP) steels, and bainite and martensite in Bainite Martensite Dual Phase (BMDP) steels, have been

A. Varshney · D. Verma · S. Sangal · K. Mondal (✉)
Department of Materials Science and Engineering, Indian Institute of Technology, Kanpur 208016, India
e-mail: kallol@iitk.ac.in

reported [16, 17]. Saeidi and Ekrami [17] have compared the FMDP with the FBDP low carbon steels. They have found higher elongation for the FBDP steels. Tomita and Okabayashi [18] have found the steel with a combination of lower bainite and martensite to result in better mechanical properties as compared to that of steel containing upper bainite and martensite. Rao [19] has patented ferrite–austenite dual phase steels with excellent mechanical properties popularly known as duplex steels obtained by a complex heat treatment. All the dual phase steels with different phases have also exhibited continuous yielding behavior [4, 6, 13–19]. Few studies [20–23] have observed decrease in all the mechanical properties and appearance of discontinuity in the stress strain curve after tempering the FMDP steels in a wide temperature range. In case of multiphase steels, transformation induced plasticity (TRIP) assisted steel with ferrite, bainite and retained austenite, which later transforms to martensite on application of strain, has been studied in detail, and commercially developed for the automobile applications [24, 25].

It is evident from the earlier studies that a considerable amount of work has been done on different combinations of phases and subsequent tempering. However, steels with pearlite-martensite and pearlite-tempered martensite combination have been studied by few researchers. Hansen and Pradhan [26] has concluded through regression analysis that martensite is a three times more effective strengthener as compared to pearlite, but has deleterious effect on both uniform and total elongation depending on volume percent of different phases in the FMDP steel, where pearlite and martensite are present as second phase. Marder [27] has shown that presence of less than 6 % pearlite and more than 12 % martensite results in continuous yielding. Effect of volume fraction of pearlite and martensite on mechanical properties has been studied as the second phase only, not as primary microstructural constituents.

In this investigation, a combination of phases i.e. pearlite and tempered martensite with ferrite in small amount has been obtained by isothermal transformation of a high carbon steel in the pearlitic region followed by water quenching and subsequent tempering. Variation of mechanical properties with volume fraction of constituent phases has been reported and analyzed. Deformation mechanisms of the multiphase steels have also been discussed.

2 Experimental Procedure

2.1 Materials Detail and Heat Treatment

Table 1 gives details of composition of the rail steel studied in the present work. The processing details of the steel are described elsewhere [28]. The steel was obtained in the form of rolled rails. The as-received rail steel had a fully pearlitic microstructure. The martensitic start temperature (M_s) was estimated to be 478 K, as calculated from the following equation [29]:

$$M_s(^\circ C) = 539 - 423(\%C) - 30.4(\%Mn) - 17.7(\%Ni) - 12.1(\%Cr) - 7.5(\%Mo,\ W,\ Si) \quad (1)$$

The rolled rail was sliced into small cuboid samples of dimension $15 \times 15 \times 5$ mm for metallographic examination and hardness measurements. For the measurement of tensile properties, the tensile samples were made and tested according to ASTM E8 M [30] standard for sub-size flat specimen with a gauge length of 25 mm. The specimen geometry is shown in Fig. 1. Flat specimens for tensile testing were preferred to ensure uniform heat treatment. In order to obtain a pearlitic-martensitic dual phase structure, all the samples were first austenitized in a muffle furnace at 1173 K for 21 min to achieve complete homogenization. The samples after complete austenitization were subjected to isothermal holding at three different temperatures (923, 933 and 938 K) in the pearlitic zone for different time durations (90–300 s) to obtain varying amounts of pearlite followed by quenching in water. After that, the quenched samples were subjected to an optimized tempering schedule.

A series of experiments was first carried out to guide the choice of optimum tempering temperature and duration. A set of tensile samples was isothermally transformed at 923 K for 120 s after homogenization at 1173 K for 21 min to get a fixed amount of pearlite (~26 %) and martensite (~74 %) before tempering at three different temperatures (623, 723 and 773 K) for various durations (8.5–18 h). Tempering temperature of 773 K and duration of 18 h were selected to optimize tempering condition after looking for the desired tensile properties. It was observed that this particular combination of tempering temperature and time (773 K and 18 h) yielded maximum elongation in combination with fairly good amount of yield and ultimate tensile strength.

After optimization of tempering temperature and time, another set of cuboid and tensile samples after complete homogenization was quenched in the salt bath maintained at 933 K and 938 K for partial isothermal transformation of austenite to pearlite. The samples were held at these temperatures for different holding durations. At 933 K, the samples were held for 90, 180 and 225 s. At 938 K, the samples were held for 240 s and 300 s. The samples were quenched to room temperature after partial pearlitic transformation. Quenching allowed untransformed austenite to transform to martensite. These samples were allowed to transform isothermally at two different temperatures for

Table 1 Composition of as-received C–Mn rail steel

Elements	C	Mn	Si	S	P
Wt%	0.71	1.04	0.21	0.013	0.022

different holding durations in pearlitic range with an objective of obtaining varied volume fractions of pearlite and martensite from the same prior austenite grain size in each case. The composition of the salt bath was 55wt% $BaCl_2$ + 25wt% KCl + 20wt% NaCl, which gave a working temperature range of 863–1,198 K. Change in the lamellar spacing of pearlite due to different transformation temperatures was not considered critically, since difference between two transformation temperatures (933 and 938 K) was not substantial.

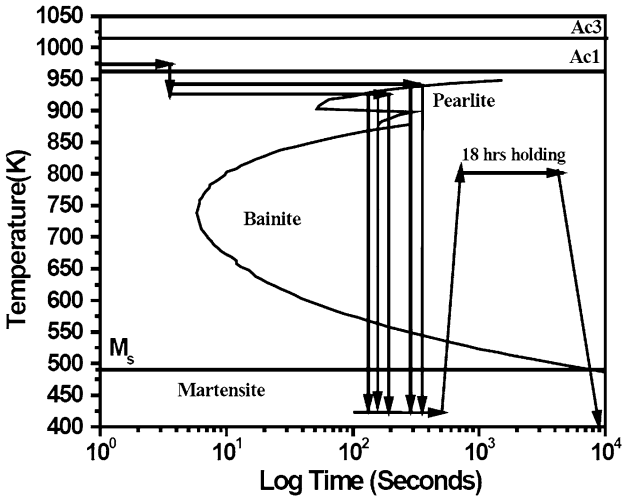

Fig. 2 Heat Treatment cycle superimposed on TTT curve employed for present work. The TTT curve is obtained by applying the program mentioned in Ref no. [31]

2.2 Sample Preparation and Microstructural Characterization

Optical microstructural examination, micro-hardness measurements and X-Ray Diffraction (XRD) of selected samples in un-tempered condition were carried out. Un-tempered samples were then tempered at 773 K for 18 h. Tempered samples were subjected to Scanning Electron Microscopic (SEM) analysis, micro-hardness measurements, XRD and tensile tests. The isothermal transformation temperatures were decided from time–temperature-transformation (TTT) plot (Fig. 2). The TTT diagram was generated using software proposed by Bhadeshia [31]. The heat treatment routes have been superimposed on the TTT plot.

Samples for the microstructural examination and hardness measurement were initially ground to sufficient depth for removal of any decarburized layer from the surface. They were then mechanically ground using emery paper down to grit number 1,000, followed by cloth polishing with 5-μm and then 1-μm alumina paste. The polished samples were etched with 2 % nital. XRD of the un-tempered and tempered sample was carried out by using Cr K_α radiation (wavelength = 2.2909 Angstorms) in a Bruker diffractometer operated at 40 kV and 30 mA with scanning rate of 0.5 degree per minute. The optical metallographic examination was carried out in Leica Microsystems DM6000 M microscope. SEM analysis was carried out using a FEI QUANTA scanning electron microscope (FEI Co., Hillsboro, OR) operated at 20 kV with secondary electron imaging mode. For quantitative analysis, volume fractions of pearlite, martensite and pro-eutectoid ferrite were measured by point count method and with help of image J, a public domain image processing software.

2.3 Hardness and Tensile Testing

Micro-hardness of individual phase was measured at a load of 200 g in Bareiss Prufgeretebau GmbH D-89610 Vicker's micro hardness tester. For each sample, 10 readings were taken in order to obtain an average hardness value. Tensile tests were carried out in a Lloyd 50 KN universal tensile testing machine at room temperature. The crosshead speed was 0.1 mm/min in order to attain a strain rate of 6.67×10^{-5} s^{-1}. 0.2 % yield strength (YS) and ultimate tensile strength (UTS) were measured from the stress–strain curve. Strain measurements were done with high

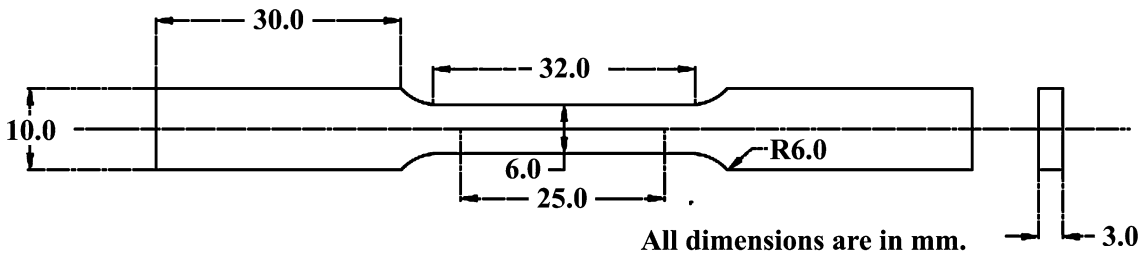

Fig. 1 Geometry and dimensions of tensile specimen used in this investigation

resolution strain gauge B-1 class extensometer. Total elongation was measured by physically joining the broken samples. SEM fractographs were recorded from fractured surfaces of the tensile specimens containing varying volume fractions of pearlite and TM. Fractographic analysis was carried out to compare the deformation mode in various tensile specimens as a function of volume fractions of constituent phases.

2.4 Analysis

Strain hardening analysis was carried out by fitting true stress- true plastic strain data to Hollomon and Ludwigson equations. Strain hardening exponent (n_H) for Hollomon equation [32] was determined as per ASTM standard E-646-98 [33]:

$$\sigma = K_H \varepsilon_p^{n_H} \tag{2}$$

where, σ and ε_p are true stress and true plastic strain, respectively [16]. K_H is the strength coefficient for hollomon's equation. The value of n_H for different tensile specimens was estimated from the slope of log–log plots of true stress (σ) versus true plastic strain (ε_p) data obtained from the tensile tests.Parameters of Ludwigson equation [37–39] (Eq. 3) were fitted on the basis of non-linear fitting by iterative method.

$$\sigma = K_L \varepsilon_p^{n_L} + e^{(K_{L1} + n_{L1}\varepsilon_p)} \tag{3}$$

where, K_L and K_{L1} are the strength coefficients while n_L and n_{L1} are the strain hardening exponents.

3 Results and Discussion

3.1 Optimization of Tempering Temperature

Table 2 shows the tensile test data for the samples isothermally held at 923 K for 120 s followed by water quenching and subsequent tempering at different temperatures (623, 723 and 773 K) for different times (8.5–18 h). It is clear that the sample, tempered at 623 K for 8.5 h, has failed in a brittle manner. The samples, tempered at 723 K for 6 and 10 h, have shown some amount of plastic deformation before failure. The elongation is noted to be in the range of 10–11 %, while the value of UTS is found to be of the order of 1,150 MPa. Subtle difference in elongation is noted, and it is slightly higher in case of the samples tempered at 773 K for 10 h with decrease in the value of UTS to ~933 MPa. Higher ductility (15 % elongation) is observed in the samples tempered at 773 K for 18 h along with slightly higher value of UTS (~967 MPa) as compared to the sample tempered for smaller durations at the same temperature.

It is to be mentioned here that prolong tempering of the order of 18 h could be a subject of concern from energy consumption. However, other factors, like use of steel with inexpensive alloying addition in small amounts and gaining very good combination of strength and ductility, can counter cost associated with prolonged tempering. The investigated steel is a standard Indian C–Mn rail steel with no costly alloying additions. Mechanical properties of the steels subjected to prolonged tempering as shown in Table 2 and 4 are far better than the as-received pearlitic steel.

Prolonged tempering is not uncommon and has been used earlier by several researchers. Hasan et al. [37] have tempered a high carbon steel for 42 days at a temperature close to 973 K. Various die forge steels have been tempered at fairly high temperatures for durations up to 300 h [38, 39]. Long tempering durations are required to coarsen and spheroidize the carbides in TM phase. Coarsening kinetics of carbides has been reported to get retarded due to high carbon content and presence of silicon and manganese [40, 41]. Since, high carbon steel with nominal additions of silicon and manganese (Table 1) has been used in the present work, a prolonged tempering was necessary to get the desired properties.

The main objective of the current work is to have a multiphase steel with high strength and good amount of ductility. After seeing the data from Table 2, tempering temperature of 773 K and duration of 18 h are considered to be the optimum condition, since it gives reasonable

Table 2 Summary of series of experiments for obtaining optimum tempering schedule

Isothermal Holding Temperature (K)	Holding Time (s)	Tempering Temp.(K)	Tempering Time (h)	YS (MPa)	UTS (MPa)	Total Elongation (%)
923	120	623	8.5	1,459	Sample broken prematurely	–
		723	6	1,022	1,158	10
			10	909	1,138	10.5
		773	10	657	933.46	11.5
			18	722	967.3	15

combination of very good ductility (15 %) along with good strength. Rest of the analysis in the paper is carried out for the samples isothermally treated at 933 and 938 K for short time followed by quenching and subsequent tempering at 773 K for 18 h.

3.2 X-Ray Diffraction (XRD)

Both tempered and un-tempered samples were subjected to XRD analysis for the determination of phases present in the samples. Figure 3a, b show XRD patterns of the samples isothermally treated at 933 K for 225 s followed by water quenching, and after subsequent tempering at 773 K for 18 h, respectively. In case of un-tempered sample, the XRD pattern (Fig. 3a) shows a predominantly ferritic microstructure along with martensite. Presence of martensite is evident from peak splitting. A cementite peak of very low intensity can also be observed indicating presence of very small amount of cementite in the microstructure of the un-tempered sample. In the tempered sample, the XRD pattern (Fig. 3b) shows two cementite peaks in addition to two dominant ferrite peaks, which are same as those of the un-tempered sample. It can also be noted that no peak splitting is observed in case of the tempered samples. Presence of cementite peaks and absence of peak splitting indicate that all the martensite, which are present after quenching and subsequent tempering, is fully tempered. No austenite peak is observed in both the tempered as well as un-tempered samples. This confirms that retained austenite, if present, is in very small quantity and below the detection limit of the XRD machine. Thus, the XRD study indicates the presence of ferrite and martensite in the un-tempered steel and predominant presence of both ferrite and cementite in the tempered samples.

3.3 Optical and SEM Characterization

Figure 4a–c show the optical micrographs of the samples, isothermally transformed to pearlite at 933 K for 90, 180 and 225 s and subsequently quenched, respectively. Figure 5a, b show the optical micrographs of the samples isothermally transformed at 938 K for 240 and 300 s and subsequent quenching, respectively. Dark etched region in the optical micrographs is pearlite. Light gray region is martensite. White region is pro-eutectoid ferrite. Martensitic grains with pro-eutectoid ferrite at the grain boundaries (as shown by arrowhead) can be observed in the sample held at 933 K for 90 s (Fig. 4a). Trace amount of pearlite can also be observed in the sample. Martensite in the form of continuous phase along with large blocks of pearlite colonies randomly distributed in the martensitic matrix can be observed in the samples isothermally transformed at 933 K for 180 s and 225 s as shown in Fig. 4b, c).

In the sample isothermally transformed at 938 K for 240 s (Fig. 5a), small islands of martensite are surrounded by matrix of large colonies of pearlite. Pearlite colonies with ferrite at the grain boundaries (as shown by arrowhead) can be observed in the sample isothermally transformed at 938 K for 300 s (Fig. 5b). In Fig. 5b, martensite cannot be observed. As expected, pearlite content can be observed to increase with increasing duration of isothermal treatment in the pearlitic zone in Figs. 4a–c and 5a, b.

Figure 6a, b shows the SEM micrographs of the sample held at 933 K for 180 s and at 938 K for 240 s followed by

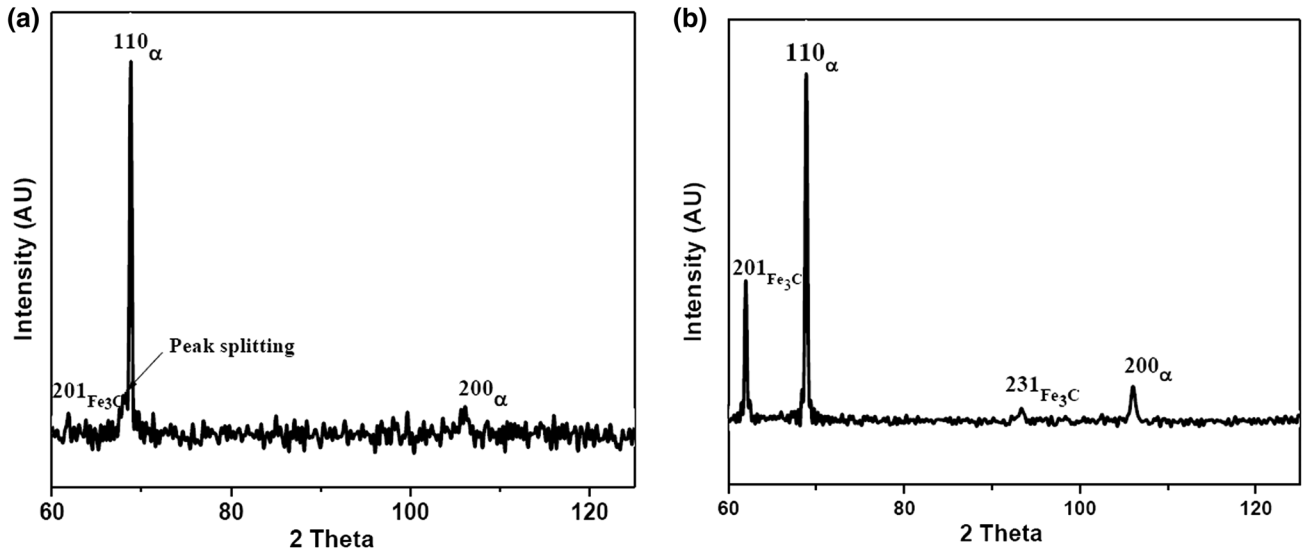

Fig. 3 XRD patterns of the steel samples isothermally transformed at 933 K for 225 s followed by (a) water quenching (un-tempered condition) and (b) water quenching and subsequent tempering at 773 K for 18 h (tempered condition)

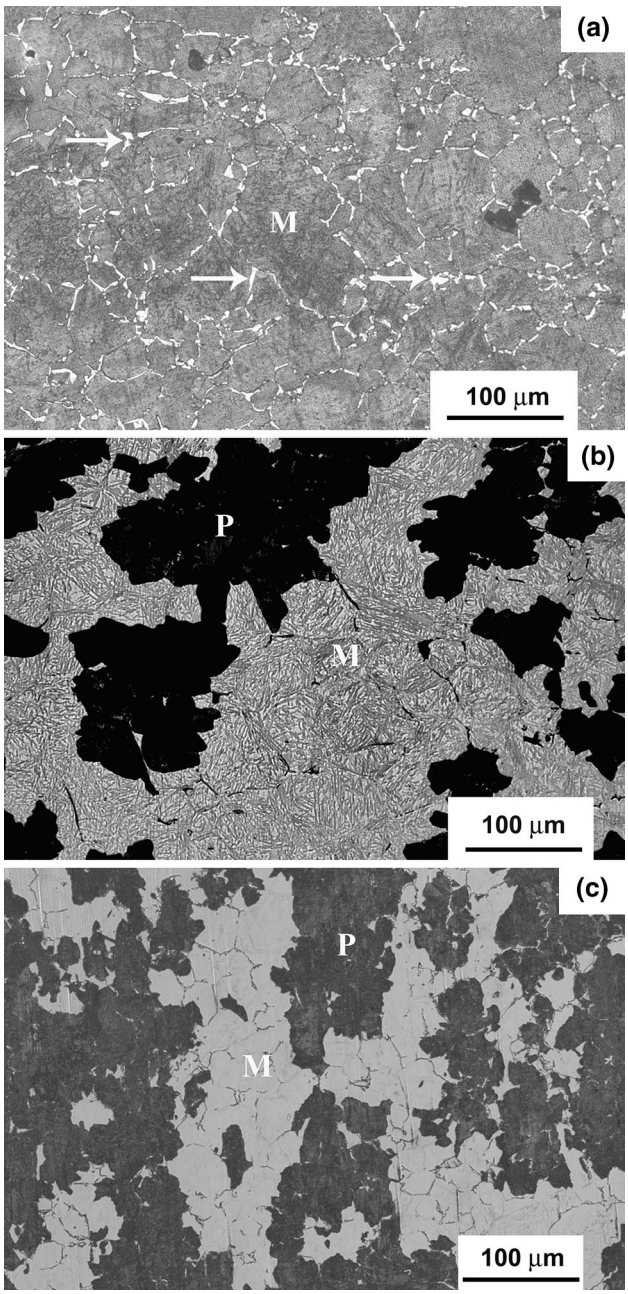

Fig. 4 Optical micrographs of the steel samples isothermally treated at 933 K for (a) 90 s (94 % martensite), (b) 180 s (72 % martensite) (c) 225 s (50 % martensite). All the samples are quenched to room temperature after treatment mentioned. (*M* Martensite, *P* Pearlite)

quenching and subsequent tempering at 773 K for 18 h, respectively Both the micrographs clearly show pro-eutectoid ferrite, pearlite and TM as the constituents of the microstructure. Both the SEM micrographs reveal the banded ferrite morphology along TM and pearlite region. As shown in Figs. 5a and 6b some blocky ferrite can also be observed. Also, TM regions are observed to be well surrounded by pearlite. Figure 7a, b show magnified SEM micrographs of the TM region of the samples held at 938 K for 240 s followed by quenching and subsequent tempering at 773 K for 18 h. These micrographs show the presence of coarse and spheroidized carbide particles as shown by arrowheads nucleated in the ferrite matrix due to a prolonged tempering treatment. Similar observations have been noticed for the sample isothermally treated at 933 K for 180 and 225 s followed by quenching and subsequent tempering at 773 K for 18 h. Presence of two carbide peaks in the XRD pattern of the sample isothermally treated at 933 K for 180 and 225 s followed by quenching and subsequent tempering at 773 K for 18 h also suggests that tempering is to some extent complete. Full tempering leads to formation of spheroidized carbides [39].

3.4 Hardness and Tensile Testing

The average micro-vicker's hardness values for different regions in un-tempered and tempered conditions are given in Table 3. Substantial difference in the hardness of martensite having value of 895 ± 7.5 HVN and pearlite having value of 299 ± 4 HVN regions can be easily observed in the un-tempered steel sample (Table 3). High hardness of martensite is due to the high carbon content (0.71 wt%) in the steel [42]. In tempered condition, hardness of martensite region has reduced to 358 ± 4 HVN along with a small reduction of hardness in pearlite to 254 ± 4 HVN. Hardness of ferrite is markedly low as compared to that of other phases in both the un- tempered and tempered samples.

Table 4 summarizes volume percent of different constituents in the samples, YS, UTS, % total elongation, total fracture strain (ε_f) and YS to UTS ratio of the investigated steel samples isothermally held for different durations at 933 and 938 K followed by quenching and subsequent tempering at 773 K for 18 h. Pearlite content can be observed to increase from ~1 to 48 % in the samples with increase in the holding duration from 90 to 225 s at 933 K. Further increase in the pearlite content from 78 to 98 % in the samples can be noted with increase in the holding duration from 240 to 300 s at 938 K. Number of pearlitic regions is observed to increase as shown in Figs. 4, 5; Table 4. With an increase in holding time of pearlite transformation temperature, the effect of increased number of pearlitic regions can be explained by following the equation developed according to Fisher hypothesis [43]:

$$I_p = I_{cm} I_f (2\pi\alpha^2) t^2 \quad (4)$$

where, I_p, I_{cm} and I_f are rate of pearlite, cementite and ferrite nucleation per unit area of austenite grain boundary, respectively. α is a constant and t is time in (s). Since rate of pearlite nucleation varies with square of time, increase in pearlite content with time is justified. YS, UTS and YS

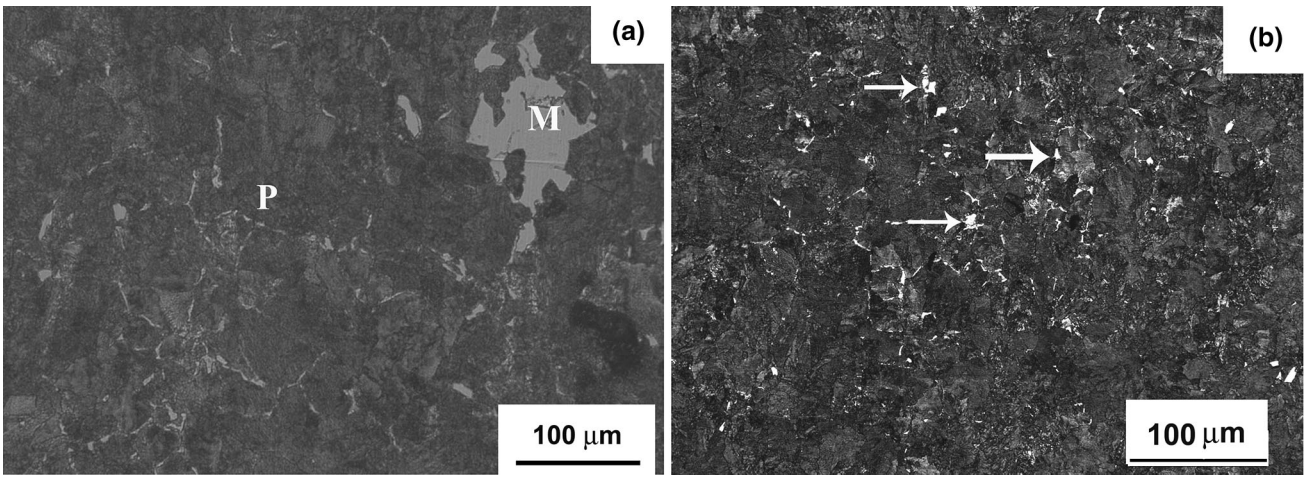

Fig. 5 Optical micrographs of the steel samples isothermally treated at 938 K for (a) 240 s (20 % martensite), (b) 300 s (no martensite). Both the samples are quenched to room temperature after treatment mentioned. (*M* Martensite, *P* Pearlite). *Arrows* show presence of ferrite at the grain boundaries of pearlite

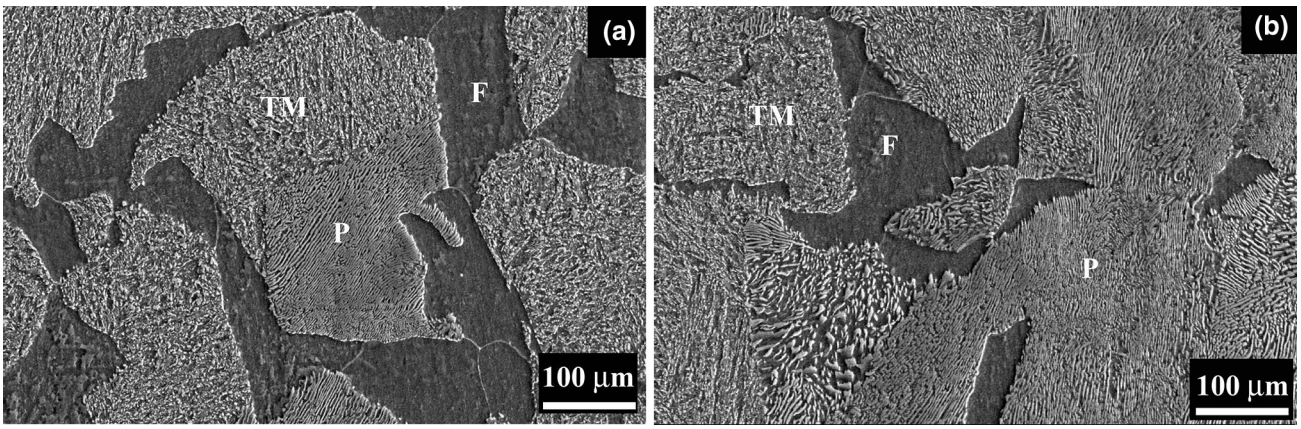

Fig. 6 SEM Micrographs showing three different phases in the steel samples held at (a) 933 K for 180 s (72 % TM) and (b) 938 K for 240 s (20 % TM) followed by water quenching to room temperature and subsequent tempering at 773 K for 18 h. Pro-eutectoid ferrite (F) can be easily seen on the grain boundaries of prior austenitic grains (tempered martensite (TM) and pearlite (P)

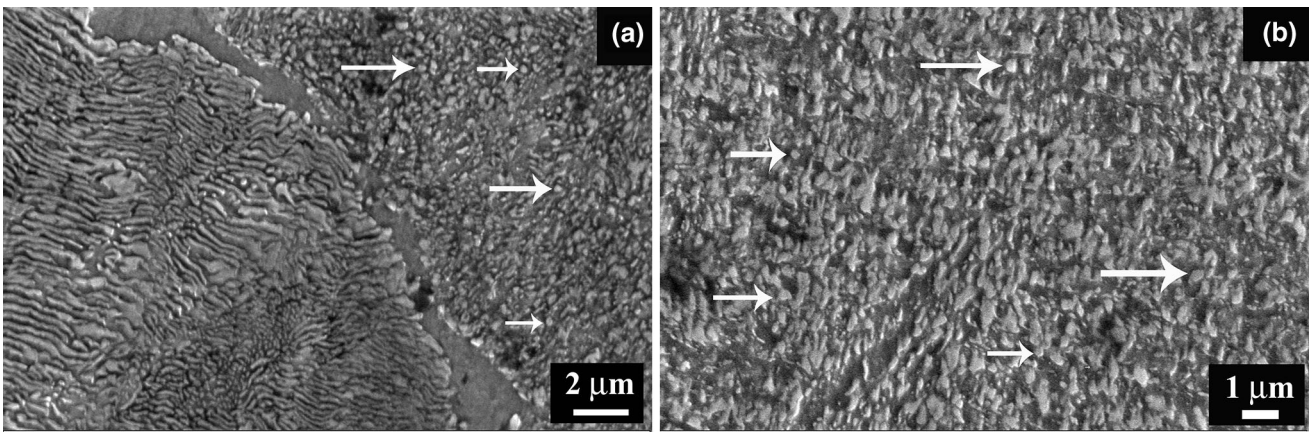

Fig. 7 Magnified SEM micrographs of the tempered martensite region in the sample held at 938 K for 240 s followed by water quenching and subsequent tempering at 773 K for 18 h. *Arrows* indicate the spheroid cementite particles in the tempered martensite region

Table 3 Average Microhardness (HVN 0.2) values of each region in un-tempered and tempered (at 773 K for 18 h) samples using a Vickers microhardness tester

	Pearlite	Martensite	Ferrite
Untempered	299 ± 4	895 ± 7.5	177 ± 5
Tempered	254 ± 5	358 ± 4	175 ± 3

to UTS ratio can also be observed to decrease with an increase in pearlite content as shown in Table 4. It is important that strain to failure is also quite high for most of the tempered steels at 773 K for 18 h as compared to the as-received rail steel suggesting improved ductility.

3.5 Yielding Behavior

Figure 8 shows typical engineering stress–strain curves for the samples tempered at 773 K for 18 h after isothermal treatment at 933 and 938 K for different durations. Each curve is characterized by the volume percent of TM obtained after heat treatment. Decrease in % elongation and increase in YS and UTS can be visibly noticed with an increase in TM content. Continuous yielding can be observed for the samples with 50, 72 and 94 % TM. Samples with 20 % TM and with fully pearlitic microstructure do not yield continuously. In this investigation, continuous yielding is referred to a smooth transition from elastic to plastic regions otherwise the yielding is understood not to be continuous. These yielding behaviors have been previously studied in detail by many investigators [44, 45].

In case of FMDP steels, the reason for continuous yielding [9, 16, 17, 42, 46–48] has been attributed to the presence of internal stresses and unpinned mobile dislocations in ferrite region around hard martensite due to the volume expansion accompanying transformation of austenite into martensite. Dislocations are unpinned in ferrite because of presence of very low amount of carbon in ferrite [16, 48]. Since, the dislocations are unpinned; ferrite phase can easily flow around hard martensitic regions and gives rise to continuous yielding [44]. Volume expansion during transformation of austenite to martensite is observed and measured by Moyer and Ansell [49]. Presence of dislocations in the vicinity of hard phase has been confirmed by Korzekwa et al. [50] through transmission electron microscopic (TEM) studies on FMDP steels.

Table 5 Values of strain hardening exponents derived from Hollomon's equation and Ludwigson's equation for samples with different tempered martensite volume percent with corresponding R^2 values

Volume percent of Tempered Martensite	n_H	R_H^2	n_L	R_L^2
0	0.195	0.967	0.482	0.991
20	0.171	0.956	0.473	0.982
50	0.154	0.988	0.34	0.998
72	0.067	0.954	0.095	0.998
94	0.054	0.910	0.075	0.995

From above discussion it is clear that for continuous yielding, unrestricted movement of dislocations is necessary. But in the present case, small fraction of soft ferrite (2–8 %) is not supposed to allow required unrestricted movement of mobile dislocations. Still, continuous yielding can be prominently observed in the samples containing high amount of tempered martensite with less ferrite. Interestingly, carbides can also be observed in tempered martensite (Figs. 3, 7a, b). It seems that if the content of tempered martensite is considerable (50–94 %), deformation is guided by the dislocation interaction with tempered martensite.

Absence of continuous yielding in the sample with 20 % TM may be due to the presence of 78 % pearlite. Carbides present as lamella as shown in Fig. 6a, b strongly restrict the motion of mobile dislocations in ferrite. This inhibits plastic flow of the ferrite phase in pearlite causing discontinuous yielding. But, continuous yielding can be noted in the sample with 50 % TM, which also has considerable amount of pearlite (48 %). Observed disparity in the

Table 4 Heat treatment schedule, Microstructural parameters and corresponding mechanical properties of the steel samples transformed at 933 and 938 K for different holding duration followed by quenching and subsequent tempering at 773 K for 18 h

Isothermal Holding Temp. (K)	Time (s)	Tempering Temp. and Time	V_{TM}^1	V_P^1	V_F^1	YS (MPa)	UTS (MPa)	UTS –YS	Total El (%)	YS/UTS
933	90		94 ± 1.5	0 ± 0.6	6 ± 1.2	1,008	1,184	174	12	0.85
	180		72 ± 2	20 ± 2.5	8 ± 2.8	900	1,035	135	13.8	0.88
	225	773 K	50 ± 3.5	48 ± 2.7	2 ± 0.5	650	940	350	16	0.68
938	240	18 h	20 ± 3	78 ± 2	2 ± 0.7	515	936	421	16.8	0.55
	300		0 ± 0.4	98 ± 1.6	2 ± 0.4	460	841	381	18	0.54
C–Mn rail steel [59, 60]		Pearlitic structure				420	890	470	12	0.47

V_{TM}, V_P, V_F = Volume percent of tempered martensite, pearlite and ferrite, respectively

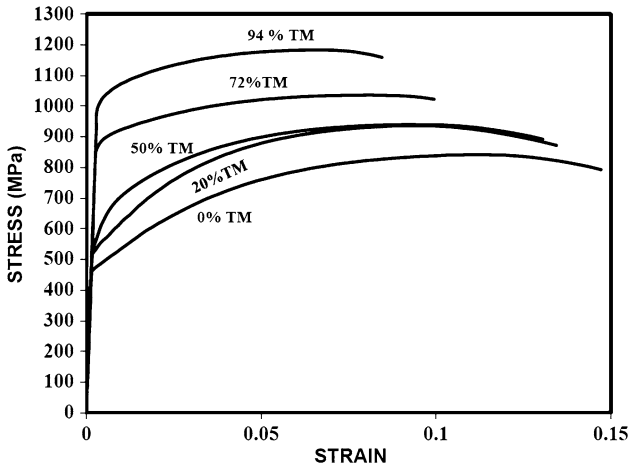

Fig. 8 Engineering stress–strain plots obtained after uni-axial tensile test of the steel samples isothermally transformed at 933 K for 90 s (V_{TM} = 94 %), 180 s (V_{TM} = 72 %), 225 s (V_{TM} = 50 %) and at 938 K for 240 s (V_{TM} = 20 %), 300 s (V_{TM} = 0 %) followed by quenching to room temperature and subsequent tempering at 773 K for 18 h. V_{TM} is volume of TM

yielding behavior may be due to domination of the flow behavior of the TM over that of pearlite. Since, the tempering schedule is same for all the steels, size of carbides formed during tempering can be assumed to be same. Thus, flow behavior of the TM phase can be assumed to be identical in all the samples. This leads to the conclusion that for a combination of TM and pearlite, there should be a critical amount of TM for the steel to yield continuously.

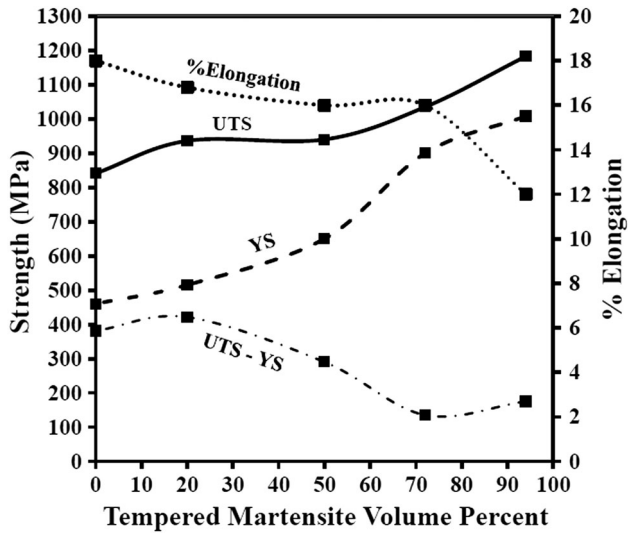

Fig. 9 Variation of tensile properties of the steel samples isothermally transformed at 933 K for 90 s (V_{TM} = 94 %), 180 s (V_{TM} = 72 %), 225 s (V_{TM} = 50 %), and at 938 K for 240 s (V_{TM} = 20 %) and 300 s (V_{TM} = 0 %) all followed by quenching and subsequent tempering at 773 K for 18 h with TM volume percent (V_{TM})

Figure 9 shows the variation of UTS, YS, % elongation and the difference between UTS and YS (UTS–YS) with TM content. Increase in YS and UTS with associated decrease in % elongation in a non-linear fashion with the increase in TM content can be easily observed. Non-linear variation of strength and ductility with respect to harder phase particles has also been reported elsewhere [16, 23, 24, 47]. Increase in YS and UTS is in conformity with the general behavior of the multiphase steels, where strength is observed to increase with increase in the volume fraction of harder phase [3–11]. This shows that both UTS and YS are sensitive to the content of hard phase. The increase in UTS is found not to vary much in the samples containing TM between 20 and 50 % as shown in Fig. 9. It can be observed that the steel samples, which show continuous yielding, have lower yield strength as compared to those showing discontinuous yielding (Fig. 8; Table 4). A lower yield strength is attributed [48] to the presence of internal stresses and plastic incompatibility between constituent phases and this probably enables yielding to take place at lower stresses.

3.6 Strain Hardening Analysis

Natural logarithm of true stress and true plastic strain has been plotted in Fig. 10a. Strain hardening exponents (n_H) corresponding to Hollomon's equation are estimated via linear regression analysis [32] and listed in Table 5 with corresponding TM content. The linear regression coefficient (R^2_H) associated with the calculation of n_H is in the range of 0.91–0.988 (Table 5). The constants in Ludwigson equation (n_L, K_L, n_{L1}, K_{L1}) have been calculated by a non-linear curve fit based on a non-linear grid search method [51] by performing number of iterations. In Table 5, values of strain hardening coefficient, n_L, are also shown. In Fig. 10b, both n_L and n_H plotted against TM volume percent show a decreasing trend with increase in the TM content. Goodness of fit for the Ludwigson equation (R^2_L) varies from 0.982 to 0.998 (Table 5). From the regression coefficient values, it is clear that Ludwigson equation describes plastic deformation of the samples in a much better way than Hollomon's equation.

Figure 11a–c show fractographs of the samples with 20, 50 and 72 % TM, respectively. Large number of brittle regions can be observed in the sample with 72 % TM as compared to those having less amount of TM. De-cohesion of the interfaces between two grains can be observed in the samples with 20 and 50 % TM as indicated by arrows in Fig. 11a, b). Figure 11c shows that this de-cohesion is minimum in the sample with 72 % TM .

It can also be observed from Fig. 9 that a low TM content with V_m = 20 %, the difference between UTS and YS is larger than for a higher TM content (V_m = 72 and

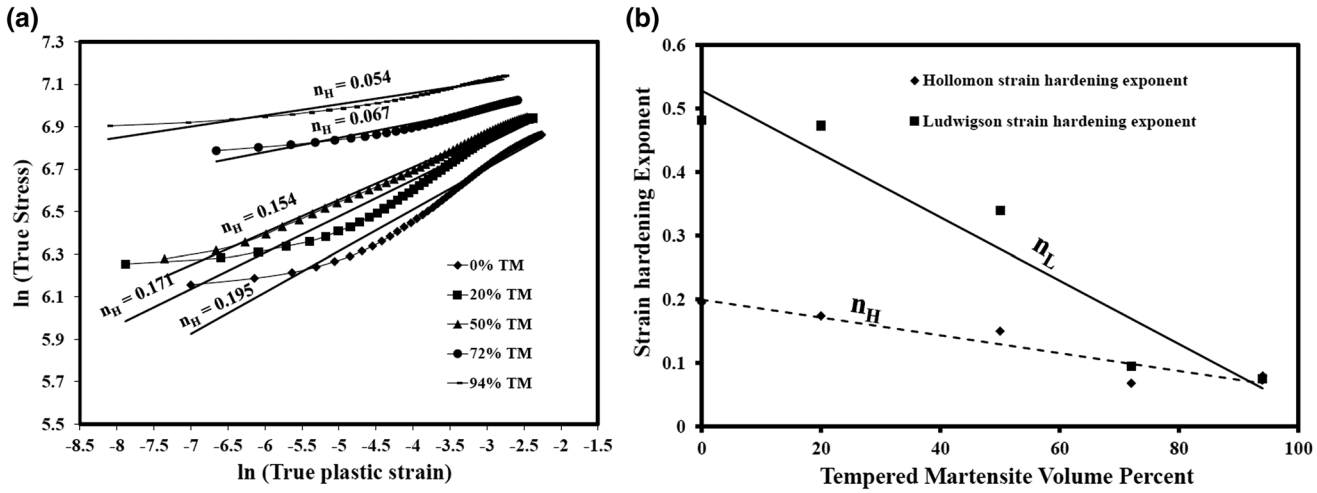

Fig. 10 (a) Plot showing the strain hardening analysis based on Hollomon's equation (Eq. 2) of the steel samples with varying volume percent of TM obtained after different heat treatment conditions as listed in Table 4. (b) Variation of strain hardening exponents (n_H and n_L) with TM volume percent obtained after fitting true stress and true plastic strain data to the Hollomon and Ludwigson equations

94 %). This is supported by high n_H and n_L values i.e. $n_H = 0.195$ and 0.17; $n_L = 0.482$ and 0.473 for the samples with no TM and 20 % TM, respectively. High values of n_H and n_L indicates high strain hardening in these samples [32]. High strain hardening in multiphase steels has been reported by other investigators also [14–16, 46, 50, 52–58]. The reason for high strain hardening in steel samples containing low volume percent of TM may be attributed to the strain partitioning between the constituent phases. Strain partitioning, on application of tensile load, usually takes place between hard and soft phases adjacent to each other [56–58].

In the present case, strain partitioning has possibly occurred between ferrite and TM due to a considerable difference in their hardness values (Table 3) and banded morphology of ferrite around the TM region as shown in Fig. 6b. But, as evident from Table 4, the volume percent of ferrite is quite low (~2 %) in the steel samples with high value of n. Hence, it can be assumed that strain partitioning would also have taken place between pearlite and TM. Since TM is surrounded by relatively softer pearlite colonies (Table 3), as evident from optical micrograph in Fig. 5a and SEM micrograph in Fig. 6b, strain partitioning between these two phases can't be denied. Thus, if strain partitioning between TM and pearlite is considered, then pearlite tends to plastically deform early as compared to TM and contribute to overall strain hardening of the steel.

Strain partitioning is also strongly supported by fractographs shown in Fig. 11. It is clear from the fractographs (Fig. 11a–c) that during tensile deformation, nucleation of crack is at the ferrite-TM or pearlite-TM interface as shown by arrowheads. The cracks are between brittle fractured region marked by river marks and region with dimple fracture. Due to strain partitioning, softer phase shares higher strain as compared to harder phase and deforms easily at the interface. The crack due to deformation is not able to propagate much through the relatively harder TM region (because of its low straining). This leads to decohesion at the interface. The nucleation of crack at the interfaces of ferrite/pearlite and martensite is also observed in an adequate work by Su and Gurland [54]. The crack grows in the softer ferrite or pearlite matrix. Plastic deformation of pearlite has been studied by Karlsson and Linden [52] who confirmed the plastic deformation of cementite lamellae through TEM and XRD analysis. To the best of authors' knowledge, combination of pearlite and TM phases has not been studied elsewhere. Therefore, detailed investigation on the strain partitioning between pearlite and TM is needed.

It can be observed from Table 4; Fig. 10b that with an increase in the content of TM (72 and 94 %), ductility and n_H and n_L values have decreased (e = 12 %, $n_H = 0.054$, $n_L = 0.075$). Figure 4a shows that this may be due to presence of very low amount of relatively soft ferrite and pearlite around TM phase. Figure 11c shows fractograph of the sample with 72 % TM also indicating minimum decohesion at the interface of the phases. Moreover, cleavage fracture is clearly observed indicating brittle fracture, and hence it leads to low elongation of 12 %, along with a small difference in UTS and YS values and low value of n_H and n_L ($n_H = 0.067$, $n_L = 0.095$) as shown in Fig. 10a; Table 5.

Finally, it can be observed that YS, UTS and % elongation in the range of 515–1,000 MPa, 900–1,184 MPa and up to 16.8, respectively, have been obtained with high n values for steel samples with low TM volume percent in Tables 4 and 5. It is to be mentioned that the main

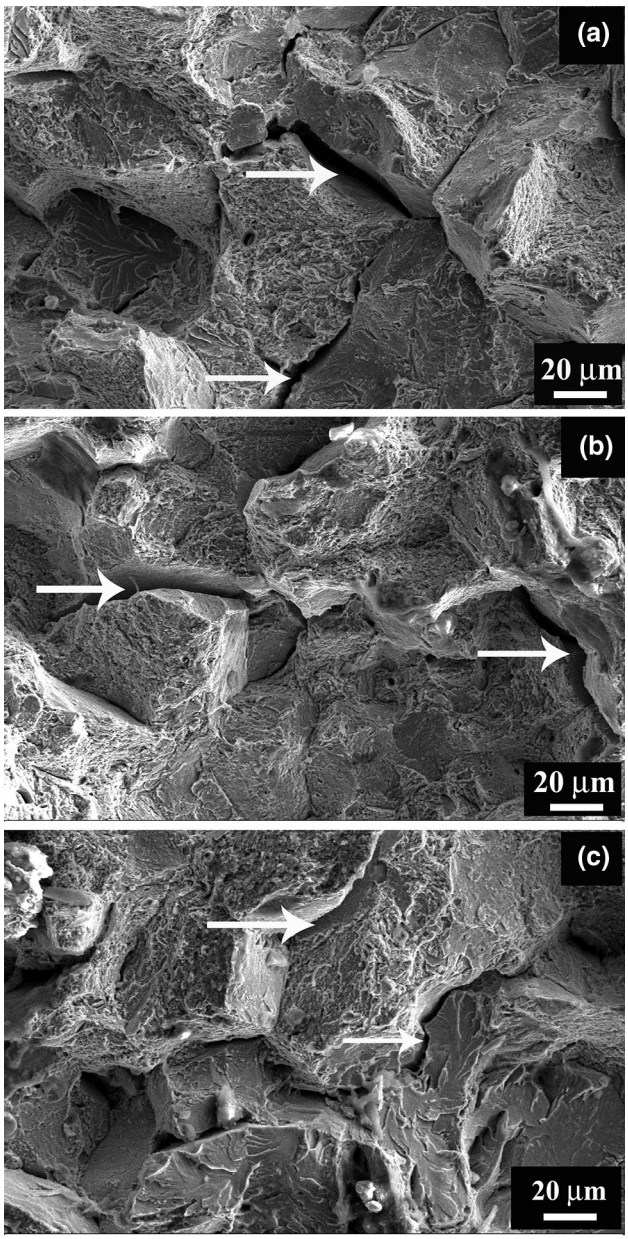

Fig. 11 SEM fractographs of the tensile tested steel samples subjected to isothermal transformation at (a) 938 K for 240 s ($V_{TM} = 20$ %), (b) 933 K for 240 s ($V_{TM} = 50$ %) and (c) 933 K for 180 s ($V_{TM} = 72$ %). All samples are quenched and subsequently tempered at 773 K for 18 h. De-cohesion regions are shown by *arrows* in (a) and (b). Minimum de-cohesion is observed in (c). (V_{TM} = Volume percent of TM)

philosophy of the present work is to see the possibility of developing a high strength steels with YS, UTS and % elongation in the range of 515–1,000 MPa, 900–1,184 MPa and up to 16.8, respectively with a combination of pearlite, tempered martensite and small fraction of pro-eutectoid ferrites from a simple high carbon-manganese steel. Even the increase in YS is more than double (YS = 1,008 MPa) in the steel sample isothermally treated at 933 K for 90 s followed by water quenching and subsequent tempering at 773 K for 18 h compared to the as received rail at the same level of % elongation. Table 4 demonstrates that he UTS is about 1,184 MPa, which is much higher than that of the as-received rail. In addition to that, the deformation characteristics of the multi-phase steels are also part of current analysis. It is interesting to note that the strength of the multi-phase steels have improved considerably with associated higher % elongation and extensive work hardening

4 Conclusions

In this work, steels with varying volume fractions of pearlite, TM and ferrite have been developed by isothermal transformation of high carbon alloy steel in diffusive range followed by quenching and tempering. Their deformation behavior has been analyzed. With increase in the holding duration at a constant temperature, pearlite content has been observed to increase. Both UTS and YS increase, while % elongation and strain hardening exponent (n) values decrease with increase in TM content. A critical amount of tempered martensite is required for the steel to yield continuously. High strain hardening and low YS to UTS ratio shown by samples with low TM content is due to a substantial strain partitioning between hard (TM) and soft regions of ferrite and pearlite. Mechanical properties of the multi-phase steels are functionally very encouraging considering that no costly alloying elements are added to these steels and simple heat treatment routes are followed.

References

1. Pickering F B, 1st edn, Chap. 9, *Controlled transformation Stainless steels*, App. Sci. Pub. Ltd., London (1978), p 197
2. Ramaswamy V, and Raghvan V, *Proc Indian Acad Sci* (*Eng Sci*) **4** (1981) 1.
3. Tamura T, Tomata Y, Akao A, Yamaoha Y, Ozawa M, and Kanotoni S, *Trans Iron Steel Inst Japan* **13** (1973) 283.
4. Hayami S, and Furukawa T, *Microalloying* **75** (1975) 78.
5. Davies R G, *Metall Trans A* **9** (1978) 671.
6. Speich G R, and Miller R L, in *Structures and Properties of Dual Phase Steels*, (eds) Kot R A, and Morris J W, New York, AIME, (1979), p 145.
7. Rashid M S, GM 980X-A unique high strength sheet steel with superior fromability SAE preprint 760206 February, Detroit, MI (1976).
8. Araki K, Takada Y, and Nakoka K, *Trans Iron Steel Inst Japan* **17** (1977) 710.
9. Eldis G T, in *Structures and Properties of Dual Phase Steels*, (eds) Kot R A, and Morris J W, AIME, New York (1979), p 202.
10. Becker J, and Hormbogen E, in *Structures and Properties of Dual Phase Steels,* (eds) Kot R A, and Morris J W), AIME, NewYork (1979), p 20.

11. Bag A, Ray K K, and Dwarakadasa E S, *Metall Mater Trans A* **30** (1999) 1193.
12. Kang S M, and Kown H, *Metall Mater Trans A* **18** (1987) 1587.
13. Das D, and Chattopadhyay P P, *J Mater Sci* **44** (2009) 2957.
14. Balliger N K, and Gladman T, *Metal Sci* **15** (1981) 95.
15. Zare A, and Ekrami A, *Mater Sci Eng A* **530** (2011) 440.
16. Kumar A, Singh S B, and Ray K K, *Mater Sci Eng A* **474** (2008) 270.
17. Saeidi N, and Ekrami A, *Mater Sci Eng A* **523** (2009) 125.
18. Tomita Y, and Okabayashi K, *Metall Trans A* **16** (1985) 73.
19. Rao B V N, Ferrite austenite dual phase steels, US Patent No. 4544422, 1 October 1985.
20. Samuel F H, *Mater Sci Eng* **75** (1985) 51.
21. Rashid M S, and Rao B V N, in *Fundamentals of Dual Phase Steels*, (eds) Kot R A, and Bramfitt B L, AIME, Pennsylvania (1981), p 249.
22. Davies R G, in *Fundamentals of Dual Phase Steels*, (eds) Kot R A, and Bramfitt B L, AIME, Pennsylvania (1981), p 265.
23. Speich G R, and Miller R A, in *Fundamentals of Dual Phase Steels*, (eds) Kot R A, and Bramfitt B L, AIME, Pennsylvania (1981), p 279.
24. Jaques P, Furnemont Q, Mertens A, and Delannay F, *Philos Mag A* **18** (2001) 1789.
25. De Cooman B C, *Curr Opin Sol State Mater Sci* **8** (2004) 285.
26. Hansen S S, and Pradhan R R, in *Fundamentals of Dual Phase*, (eds) Kot R A, and Bramfitt B L, AIME, Pennsylvania (1981), p 113.
27. Marder A R, in *Fundamentals of Dual Phase Steels*, (eds) Kot R A, and Bramfitt B L, AIME, Pennsylvania (1981), p 145.
28. Moon A P, Balasubramanium R, and Panda B, *Mater Sci Eng A* **527** (2010) 3259.
29. Sharma S, Sangal S, and Mondal K, *Metall Mater Trans A* **42** (2011) 3921.
30. ASTM, Standard Test Methods for tension testing of metallic materials E8 M, ASTM, Philadelphia, PA, USA, 1999.
31. Bhadeshia H K D H, in Materials Algorithm Project. www.msm.cam.ac.uk/map/steel/programs/mucg46-b.html.
32. Dieter G E, *Mechanical Metallurgy*, Chap. 8, McGraw—Hill Book Company, London (1988), p 287.
33. ASTM, Standard Test Method for Tensile Strain Hardening exponents (n- values) of metallic sheet materials, E-646, ASTM, Philadelphia (1999).
34. Hasan H S, Peet M J, and Bhadeshia H K D H, *Int J Mater Res* **103** (2012) 1.
35. Virtanen E, Van Tyne C J, Levy B S, and Brada G, *J Mater Process Technol* **213** (2013) 1364.
36. Zhou Q, Wu X, Shi N, Li J, Minm Na, *Mater Sci Eng A* **528** (2011) 5696
37. Choudhary B K, Rao Palaparti D P, Isaac Samuel E, Srinivasan V S and Mathew M D, *Mater Sci Eng A* **538** (2012) 110.
38. Choudhary B K, Christopher J, Rao Palaparti D P, Isaac Samuel E and Mathew M D, *Mater Des* **52** (2013) 58.
39. Christopher J, Choudhary B K, Isaac Samuel E, Mathew M D, and Jayakumar T, *J Nucl Mater* **420** (2012) 583.
40. Lindsley B A, and Marder A R, *Acta Mater* **46** (1998) 341.
41. Miyamoto G, Oh J C, Hono K, Furuhara T, and Maki T, *Acta Mater* **55** (2007) 5027.
42. Karlsson B, and Sundstrom B O, *Mater Sci Eng A* **16** (1974) 161.
43. Raghvan V, *Solid State Phase Transformations*, 2nd edn, Vol.1, Prentice Hall India Pvt. Ltd, New Delhi (1988), p 109.
44. Hahn G T, *Acta metall* **17** (1962) 727.
45. Grushko B, and Weiss B-Z, *Scr Metall* **23** (1989) 865.
46. Lanzilloto C A N, and Pickering F B, *Metal Sci* **16** (1982) 371.
47. Jena A K, and Chaturvedi M C, *Mater Sci Eng A* **100** (1988) 1.
48. Sangal S, *Room Temperature Deformation Behaviour of Multi-phase Materials with special reference to Dual Phase Steels*, M.S.Thesis, University of Manitoba, Canada (1985), p 25
49. Moyer J M, and Ansell G S, *Metall Trans A* **6** (1975) 1785.
50. Korzekwa D A, Matlock D K, and Krauss G, *Metall Trans A* **15** (1984) 1221.
51. Bevington P R, and Robinson D K, *Data Reduction and Error analysis for the physical sciences*, 3rd edn, vol.1, Mac Graw Hill, New Delhi (2003), p 151.
52. Karlsson B and Linden G, *Mater Sci Eng* **17** (1975) 209.
53. Goel N C, Sangal S, and Tangri K, *Metall Trans A* **16** (1985) 2013.
54. Su Y L, and Gurland J, *Mater Sci Eng* **95** (1987) 151.
55. Cho K, and Gurland J, *Metall Trans A* **19** (1988) 2027.
56. Woo W, Em VT, Kim E Y, Han S H, Han Y S and Choi S H, *Acta Mater* **60** (2012) 6972.
57. Marteau J, Haddadi H, and Bouvier S, *Exp Mech* **53** (2013) 427.
58. Ramazani A, Pinard P T, Richter S, Schwerdt A and Prahl U, *Comput Mater Sci* **80** (2013) 134.
59. Moon A P, Mahapatra S, Manuwal A K, Bhattacharyya A, Srikanth K and Rathi R K, *Curr Sci* **100** (2011) 52.
60. Panda B, Balasubramaniam R and Dwivedi G, *Corros Sci* **50** (2008) 1684.